



The small-size laser shock adhesive-clinching of Al foils

Yiqun Wang¹ · Guoxin Lu¹ · Zhong Ji¹ · Ren Liu¹ · Chao Zheng¹

Received: 24 February 2022 / Accepted: 6 September 2022 / Published online: 17 September 2022
© The Author(s), under exclusive licence to Springer-Verlag London Ltd., part of Springer Nature 2022

Abstract

The laser shock adhesive-clinching (LSAC) is an original material joining technique that combines the advantages of clinch-bonded hybrid joining and laser shock clinching, in which two metal foils are bonded by adhesive and clinched by laser shock simultaneously. In this paper, the LSAC joints are manufactured by 1060 Al foils, Henkel EP 5055 adhesive, and perforated 304 stainless steel sheets. Through experiments and FEM simulations, the LSAC process and the deformation of LSAC joints under shear loads are analyzed, and the effect of adhesive on LSAC joint manufacturing is investigated. The results show that bulging is the dominant deformation behavior during LASC, and the cured adhesive with thin thickness is beneficial to the subsequent clinching process. The shear strength of the LSAC joint is greatly enhanced compared to the pure clinched and pure bonded joints. The shear failure process of the LSAC joint is adhesive degumming first, then the interlock separating.

Keywords Laser shock forming · Laser shock adhesive-clinching · FEM simulation · Joint strength, Failure analysis

1 Introduction

With the rapid development of modern industry, lightweight design has attracted increasing attention [1]. Innovative joining technologies for multi-material structures as effective ways of structural lightweight have great demands in automobile, aviation, high-speed rail, and electronics [2]. Chemical bonding [3] and mechanical clinching [4] are important joining methods and have been shown to be increasingly irreplaceable, due to their easy connection for dissimilar materials with different melting points and joining properties.

However, the limitations of single joining techniques make them difficult to meet the complex requirements in many cases, such as the temperature sensitivity of adhesive bonding and the limited joining strength and corrosion resistance of mechanical clinching. Therefore, more and more people are focusing on the hybrid joining technologies that combine two or more joining methods in recent years. Among them, the clinch-bonded hybrid (CBH) joining with

both the advantages of bonding and clinching has become the most popular in the field of joining dissimilar materials [5, 6].

Early in 1989, Wines [7] used galvanized steel and polyurethane adhesive to make clinched joints with adhesive between the sheets. The shear strength and peel strength of the hybrid joint are lower than the accumulation of that of clinched joint and adhesive bonded joint under the same conditions.

Over the years, scientific research on CBH joining kept developing. He [8] found that the failure modes of clinched joints in the shear test can be neck fracture or button separation, while that of CBH joints is only neck fracture since the metal sheets have been strongly bonded. The maximum load and energy absorption of the hybrid joint is higher than the clinched joint. The shear strength of the CBH joint is mainly provided by adhesive bonding, while the peel strength is provided by clinching [9]. The adhesive makes the failure process of hybrid joints into two stages as shown in Fig. 1: adhesive failure first then followed by the interlock failure [10, 11]. Such a multi-stage failure process is beneficial to increasing the deformation limit and energy absorption capacity of hybrid joints.

The types and characteristics of adhesive have important influences on the hybrid joining. Moroni [12] used a thermosetting and tough epoxy adhesive Terokal 5077 in making CBH joints. Unidirectional tensile test results showed

✉ Zhong Ji
jizhong@sdu.edu.cn

¹ Key Laboratory for Liquid-Solid Structural Evolution and Processing of Materials (MOE), School of Materials Science and Engineering, Shandong University, 17923 Jingshi Road, Jinan, Shandong 250061, People's Republic of China

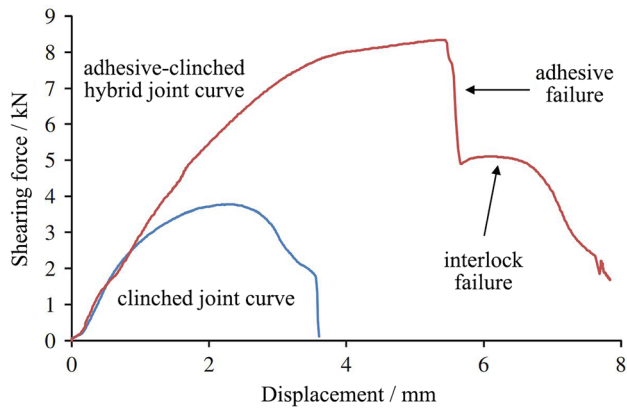


Fig. 1 Experimental load–displacement curves (for clinched, adhesive, and hybrid joints) of steel-copper joints [11]

that the shear strength of the hybrid joint is mainly provided by adhesive, and its energy absorption capacity was higher than that of pure clinched and pure bonded joints. Balawender [13] selected Draogon[®], also an epoxy adhesive but with obvious brittleness after curing to make CBH joints, as shown in Fig. 2, and observed local failure of the adhesive near the interlock structure, which was induced by the slight damage of the cured adhesive during clinching process.

As a metal sheet joining technology, the strength of the CBH joint is also affected by many external factors, such as material aging, environmental corrosion, and metal fatigue. With the extension of working time, the aging of adhesive will adversely affect the joint strength. Pinger [14] conducted a 2-year outdoor placement experiment of clinched, bonded, and CBH joints using galvanized steel sheet and found that the adhesive aging led to the reduction of shear strength in the hybrid joints and bonded joints, while the clinched joints have no significant change. Because the adhesive is coated between the two layers of materials to be connected, the contact between different sheets is fully isolated. When the different sheets are connected, the barrier effect of adhesive can significantly improve the corrosion resistance of the joint as shown in Fig. 3 [15].

Fig. 2 The cross-sections of the CBH joints [13]: **a** brass-copper joint, **b** steel-brass joint, **c** steel-copper joint

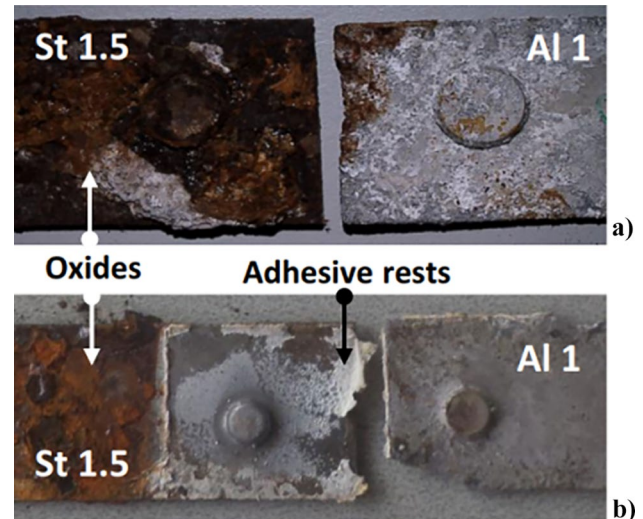
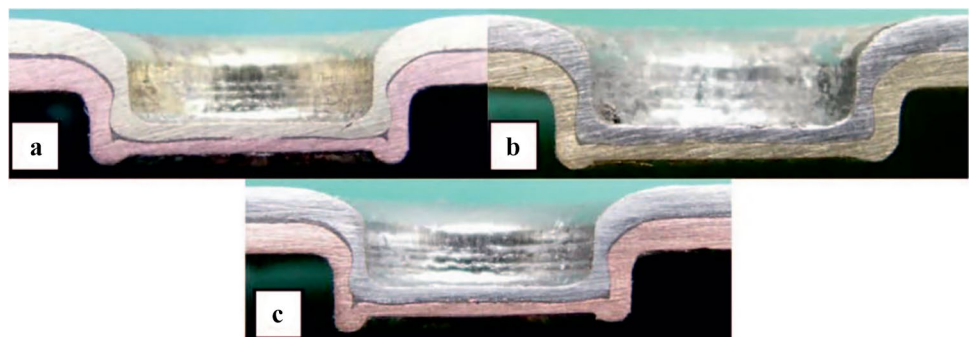


Fig. 3 Comparison of failure surface of the St1.5/Al1 joints at aging 5 weeks [15]: **a** without adhesive and **b** with adhesive

In addition to the improvement of joint performance, the adhesive also has an important effect on the forming process of the hybrid joint. Xing [16] and Liu [17] found that viscous adhesives have a certain lubrication effect, which can reduce the friction resistance between sheets. Friedrich [18, 19] found that applying adhesives under heating conditions during the clinching process can increase the shear and peel strength of hybrid joints. Zhuang [20] investigated the influence of viscosity on the forming process, mechanical strength, and failure mode of hybrid joints with dissimilar materials by controlling the proportion of adhesive curing.

Due to the complex deformation and interaction between materials with different physical properties, using finite element method (FEM) to simulate the forming and failure process of hybrid joints can effectively obtain detailed mechanical information and help to understand the deformation mechanism of metal sheets and adhesives. Pironi [21] simulated the tensile shear test of clinched and CBH joints by the arbitrary Lagrangian–Eulerian (ALE) algorithm. Gurson–Tvergaard–Needleman (GTN) model and Cohesive-Zone (CZ) model were used to simulate the

metal and adhesive damage respectively. Balawender [22] attempted to define the damage of Pattex® epoxy adhesive by using a secondary stress criterion:

$$\left(\frac{t_n}{t_n^0}\right)^2 + \left(\frac{t_s}{t_s^0}\right)^2 + \left(\frac{t_t}{t_t^0}\right)^2 = 1 \quad (1)$$

where t_n^0 , t_s^0 , and t_t^0 are the peak values of nominal stresses when the three-directional deformation occurs along the adhesive section. FEM results showed that the adhesive in the clinching area will be damaged when performing the clinching process after the adhesive is cured. Sadowski [23] found that the strength of the hybrid joint was lower than the experimental result, which may be caused by the undefined strengthening effect of adhesive on interlock structure. Fricke [24–26] used the ALE algorithm to simulate the forming process of the CBH joint and to explore the influence of adhesive viscosity. The segregation and redistribution of the adhesive lead to the formation of “adhesive pockets,” which is a typical local converging behavior. The higher the viscosity of the adhesive, the larger the size of the adhesive pocket formed.

The idea of laser shock clinching (LSC) was originally presented by Ji [27]; the laser-induced shock wave was used as a flexible punch to form clinched joints of thin metal foils. Vollertsen [28–31] realized such technique using aluminum foils, perforated steel sheets, and a TEA-CO₂ laser. Zheng [32] studied the deformation behavior and failure mode of copper-steel LSC joints. The thermal effect of laser beam is not obvious on the copper foils. The laser energy density affects the laser energy threshold and the number of pulses required for forming foil interlock structure.

Wang [33–35] added a layer of polyurethane rubber material in the LSC technique for better conduction of laser shock wave pressure and studied the influence of ablator layer, rubber, die depth, and laser energy on aluminum-copper foil

LSC joints. Different laser energies need different thicknesses of ablator layer; the force of laser shock on metal foil increases first and then decreases with the increase of ablator layer thickness. An LSC joint with high quality and connection strength is supposed to ensure sufficient interlocking depth and joint neck thickness at the same time. Higher laser energy leads to deeper the interlocking depth, but will also cause thickness reduction of the foils at the joint neck and bottom.

In addition to the research above, Vollertsen applied LSC to make metal–glass and metal–plastic joints [36, 37], Ji [38–42] achieved round and rectangular double-layer LSC joints as shown in Fig. 4 and have all made significant contributions to the development of LSC technologies.

However, there are still some problems to be solved with the two joining techniques. For the current clinch-bonded hybrid joining, metal sheets of mm-level thickness and above are the most common object, and the volume of adhesive is far less than that of metal sheets, and its effect on CBH joint forming can be negligible in most cases. When it comes to metal foils of μm -thickness, the co-interaction between metal foils and adhesive remains to be explored. Besides, by laser shocking technique, the size of CBH joints can be made smaller, and with its advantages in sealing and corrosion resistance, this process can have great significance and prospects in electronic component manufacturing.

In this paper, an original technique named laser shock adhesive-clinching (LSAC) is put forward, in which two Al foils are bonded by adhesive and clinched together by laser shock. The forming and failure process of LSAC joints are investigated by experiment and FEM simulation. Shear tests are carried out to contrast the joint strengths of hybrid, pure clinched, and pure bonded joints. The effects of adhesive and its parameters on LSAC joint forming are discussed in detail. LSAC fits with the purpose of lightweight design, provides a new way for multi-material connection, realizes

Fig. 4 LSC joints: **a** single-layer spot-clinching [38], **b** double-layer spot-clinching [39], **c** double-layer line-clinching [42]

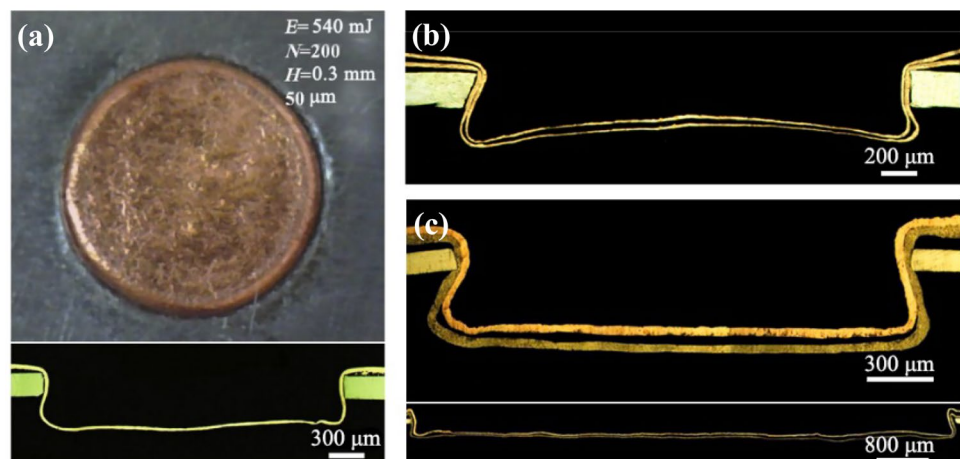
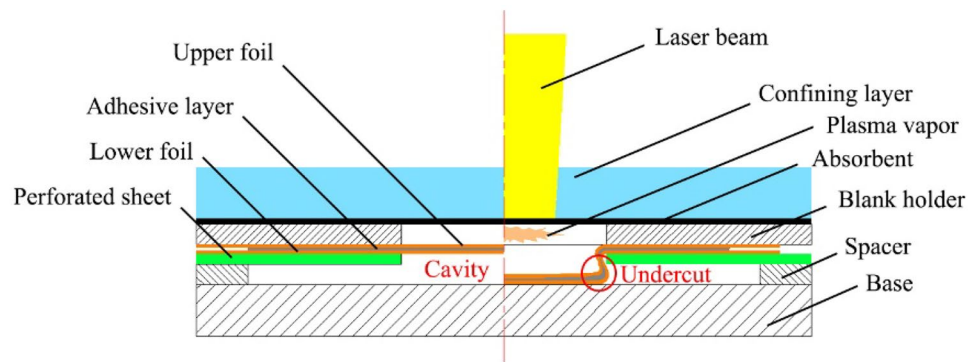


Fig. 5 Schematic of LSAC



the clinch-bonded hybrid joining of similar or dissimilar foils, and has great potentials in microscale manufacturing and electronic industries.

2 Experiments

2.1 Experimental mechanism

LSAC uses the shock wave induced by short-pulse laser to have the pre-gummed foil-adhesive-foil structure clinched. Its devices are as shown in Fig. 5, including laser beam, confining layer, absorbent, blank holder, spacer, and base. The materials to be connected in this work include two layers of metal foil, an adhesive layer, and a perforated sheet. The appearance of the finished hybrid joint looks like a circular button. The purpose of introducing a confining layer is to restrict the propagation of explosive plasma and to create a high-amplitude pressure which forces the foils into the cavity.

After gumming, the two foils are clamped between the blank holder and the spacer, and the center of the gummed area is aligned with the center of the laser beam spot. As the laser shock number increases, the two foils and the adhesive gradually bulge towards the base and flow into the cavity through the hole on the perforated sheet, then radially deform into an undercut when the lower foil touches the base. Finally, mechanical clinching and adhesive bonding between two layers of foil are completed; meanwhile, there is also interlocking between the two foils and perforated sheet. In the actual processing, the perforated sheet can be removed according to demand.

2.2 Specimen preparation

The laser generator used in this paper is Nd:YAG short-pulse laser, and the diameter of the laser spot is adjusted to 5 mm. A 3-mm-thick K9 glass sheet is applied as the confining

layer for high strength, good light transmittance, and no obvious energy weakening when the laser passes through. The absorbent is carbon black extracted from prepared Chinese ink, which is easily vaporizing and ionizing and does not react with the materials to be connected.

According to the application of LSAC, 1060 aluminum is chosen due to its good ductility and is widely used in electronic device manufacturing. To ensure that no obvious deformation occurs on the perforated sheet under laser shocking, 304 stainless steel is applied as the sheet material since its mechanical strength is far larger than 1060 aluminum. The Henkel EP 5055 epoxy structural adhesive is adopted, which has the advantages of high strength, high toughness, corrosion resistance, and wide applicability. Its initial curing condition is 4 h at 23 °C, and the complete curing condition is 48 h at 23 °C or 0.5 h when heated to 100 °C.

Lap specimens of LSAC joints are manufactured for the shear tests; each parameter combination has been made 5 specimens for reducing error. Schematic and dimensions of the test joints are shown in Fig. 6 and Table 1, respectively. To cure adhesive and release residual stress completely, each specimen is tested or observed 48 h after manufacturing.

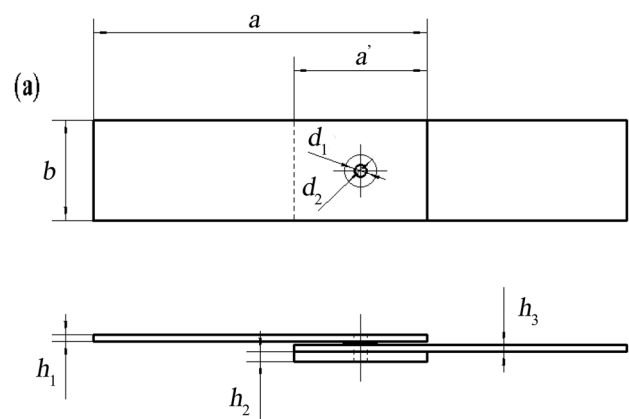


Fig. 6 Schematic of lap joint for the shear test

Table 1 Dimension of joint and mold system

Dimension	Value/mm
Foil length a	50
Foil width b	15
Foil overlapping length a'	20
Perforated hole diameter d_1	2
Adhesive gumming diameter d_2	5
Foil thickness h_1	0.03
Adhesive gumming thickness h_2	0.01
Perforated sheet thickness h_3	0.1

2.3 Key techniques of FEM

2.3.1 Finite element modeling

To acquire the mechanical information of the “foil-adhesive-foil” structure and explore the interaction between foil and adhesive during laser shocking, and also the failure behavior of LSAC joints in shear tests, FEM is used to simulate the LSAC joint forming and failure process. Since the characteristic size of the LSAC joint is much larger than the thicknesses of materials, the LSAC joint is modeled by shell elements to reduce calculation time. The blank holder and base are defined as rigid bodies since they are not involved in deformation. The perforated stainless steel sheet is also considered as a rigid body because its mechanical strength is much larger than the Al foils, and hardly deforms during laser shocking according to the experiment results.

2.3.2 Laser shock wave simplifying

The thermal effect of the laser on the connecting materials can be neglected because of the protection of the absorbent;

thus, the laser shock process can be simplified to a pure pressure loading process, which is described by Fabbro’s pressure model [43]. Since the action time of a single laser pulse is extremely short, for reducing calculation, the shock pressure is simplified to a triangular wave, as shown in Fig. 7a, which reaches the peak at one laser pulse duration τ and declines to zero at 3τ , and this shock pressure obeys Gaussian spatial distribution [32], as Fig. 7b illustrates.

2.3.3 Constitutive model of materials to be connected

In this work, the Johnson–Cook (J-C) [44] constitutive model, which is widely adopted in high-strain-rate processing such as laser shock forming, is applied to describe the deformation behaviors of 1060 aluminum.

$$\sigma_y = (A + B\varepsilon^n) \left(1 + c \ln \frac{\dot{\varepsilon}}{\dot{\varepsilon}_0} \right) \left[1 - \left(\frac{T - T_r}{T_m - T_r} \right)^m \right] \quad (2)$$

where σ_y is the effective yield strength of the material; ε is effective plastic strain, $\dot{\varepsilon}$ and $\dot{\varepsilon}_0$ are effective strain rate and reference effective strain rate; T , T_r , and T_m are environment temperature, room temperature, and the material melting temperature, respectively; A is the initial yield stress of the material, B is the hardening constant, C is the strain rate constant, N is the hardening index, and M is the thermal softening index. The constants of 1060 aluminum are shown in Table 2 [42].

The cured adhesive is an elastoplastic material; however, since its strength is much lower compared to the 1060 Al, its rate effect was neglected. The basic material properties of Henkel EP 5055 adhesive after curing are given in its operation manual [45], as shown in Table 3. Tensile tests are carried out using casted I-shaped cured adhesive specimens according to the Chinese national standard GB/T 10,402–2006, and the stress–strain curves obtained are

Fig. 7 Simplified laser shock wave [32]: **a** temporal distribution, **b** spatial distribution

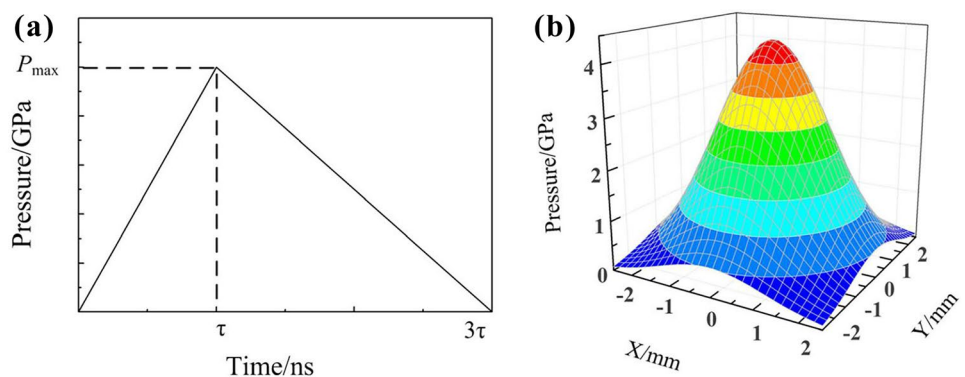


Table 2 The constants of 1060 Al in the J-C constitutive model [42]

A/MPa	B/MPa	c	n	m	T_r	T_m
148.4	345.5	0.001	0.183	0.895	293	916

Table 3 Mechanical properties of cured Henkel EP 5055 adhesive [45]

Density/g cm ⁻³	Young's modulus/MPa	Shear strength/MPa	Peel test/N mm ⁻¹
1.05	1500	> 20	> 4

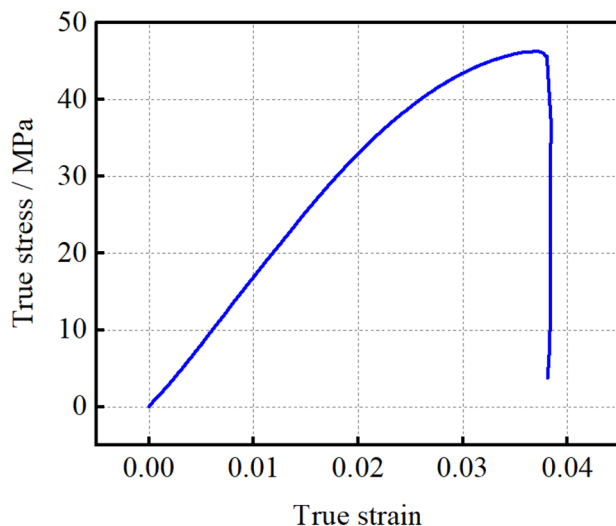
shown in Fig. 8. Based on the data in Table 3 and Fig. 8, the constitutive model of adhesive is established.

3 Results and discussion

3.1 Manufacturing of LSAC joint

Figure 9 shows the section view and surface morphology of the aluminum-adhesive-aluminum-stainless steel (Al/Ad/Al/Ss) LSAC joint. The thicknesses of the Al foil, adhesive, and perforated sheet are 30 μm , 10 μm , and 0.1 mm, respectively. The hole diameter on the perforated sheet is 2 mm, the forming height H is 0.3 mm which is equal to the height of the spacer. The laser pulse duration τ is 8 ns, its energy E is 280 mJ with the spot diameter of 5 mm, and the laser shock number is 60.

As Fig. 9a shows, the two foils and the adhesive are successfully clinched into the hole on the perforated sheet, and the foil thickness in the button has reduced obviously, especially at the button corner, which means that bulging is the dominant deformation behavior during LASC. Under laser shocking, the adhesive redistributes and forms adhesive pockets. In this paper, the interlocking depth is defined as the horizontal distance between upper and lower foils, and between lower foil and perforated sheet, as shown in Fig. 9a. The former interlocking depth 36.1 μm is smaller

**Fig. 8** True stress–strain curve of cured Henkel EP 5055 adhesive

than the latter 27.1 μm since an adhesive pocket has occupied a certain space. The larger the adhesive pocket is, the more size difference between the two interlock structures will be. Figure 9b shows the morphology of the front surface of the joint, and the rolling texture inside the button area has disappeared due to the laser shock, while that outside the button is still clear. Figure 9c exhibits the exaggerated view of adhesive in the circle of (a). It can be observed that the adhesive has good wetting properties and close bonds to the surface of foils. No degumming occurs after laser shock. In addition, small fluctuations of the upper foil caused by so many times laser shock can be observed.

Figure 10 contrasts the section views of LSAC joint at different forming stages by experiment and FEM simulation; laser shock numbers from (a) to (f) are 10 to 60 respectively, and the other parameters are the same as above. With the increase of the laser shock number N , two foils and adhesive flow into the cavity first; after contacting the base, the whole structure bulges along the axial direction and finally forms the interlock structure between upper and lower foil, lower foil, and perforated sheet. Higher stresses mainly concentrate at the bottom and the button corner. The stress of adhesive is much lower than the two foils, and the stress of the lower foil is lower than that of the upper foil. Such a phenomenon indicates that the adhesive can have a cushion effect, which homogenizes the laser shock force as it passes through the upper foil and the adhesive.

3.2 Effect of adhesive on LSAC

Henkel EP 5055 is a two-component epoxy adhesive; its viscosity-time relationship at 20 $^{\circ}\text{C}$ is shown in Fig. 11 [46]. To explore the effect of adhesive viscosity on LSAC, the curing times of the adhesive in LSAC joints are controlled. The

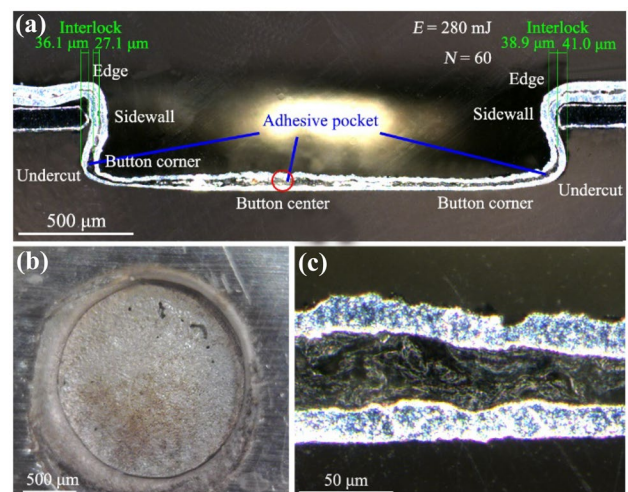
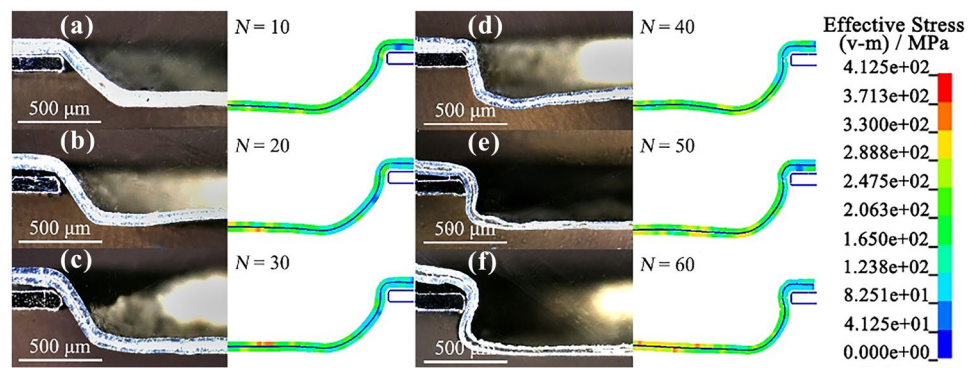
**Fig. 9** Al/Ad/Al/Ss hybrid joint: **a** cross-section view, **b** morphology of laser shock side, and **c** exaggerated view in the circle of **a**

Fig. 10 Experimental and simulated forming process of LSAC joint: **a** 10, **b** 20 **c**, 30 **d**, 40, **e** 50 **f** 60



thickness of Al foils, adhesive layer, and perforated sheet is 30 μm, 10 μm, and 0.1 mm, respectively; the laser energy E is 280 mJ, spot diameter is 5 mm, and laser shock number N is 60; the forming height H is 0.2 mm. Section views of LSAC joints under different adhesive curing times T are shown in Fig. 12.

When processed immediately after mixing without curing, the adhesive is still in the viscous flow state and easily redistributes under laser shock force, resulting in the poor forming quality of LSAC joint and even foil fracture, as shown in Fig. 12a. As curing time T increases from (b) to (e), the forming quality of the LSAC joint is improved, the adhesive distribution between two foils is uniform, and no large adhesive pockets appear. It should be noted that although the adhesive curing time T is different from (b) to (e), the joint structures are almost the same, which proves that after reaching a certain degree, the adhesive viscosity has little effect on the forming of LSAC joint.

For exploring the effect of adhesive thickness on LSAC, joints with different adhesive thicknesses are manufactured and as shown in Fig. 13. The thickness of foils and perforated sheets is 30 μm and 0.1 mm; forming height H is 0.3 mm; laser energy E is 280 mJ, and the laser spot diameter is 5 mm. Laser shock is conducted after adhesive curing. As shown

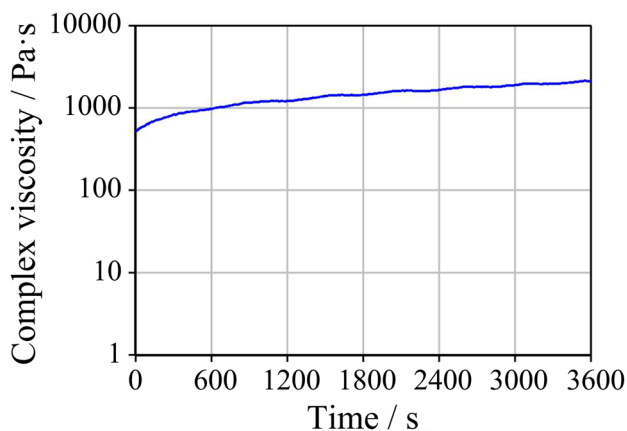


Fig. 11 Viscosity-time curve of Henkel EP 5055 adhesive at 20 °C [46]

in Fig. 13a, when applying an adhesive in 5 μm thick, the whole joint is well manufactured, and no obvious adhesive pockets appear even at the undercut. When applying adhesive with a middle thickness (about 10 μm), adhesive redistributes and gathers to pockets at the bottom and the undercut, as shown in Fig. 13b. When the adhesive layer is thick (about 20 μm), the joint cannot be formed successfully because of the excess adhesive. Plenty of adhesive gathers at bottom of

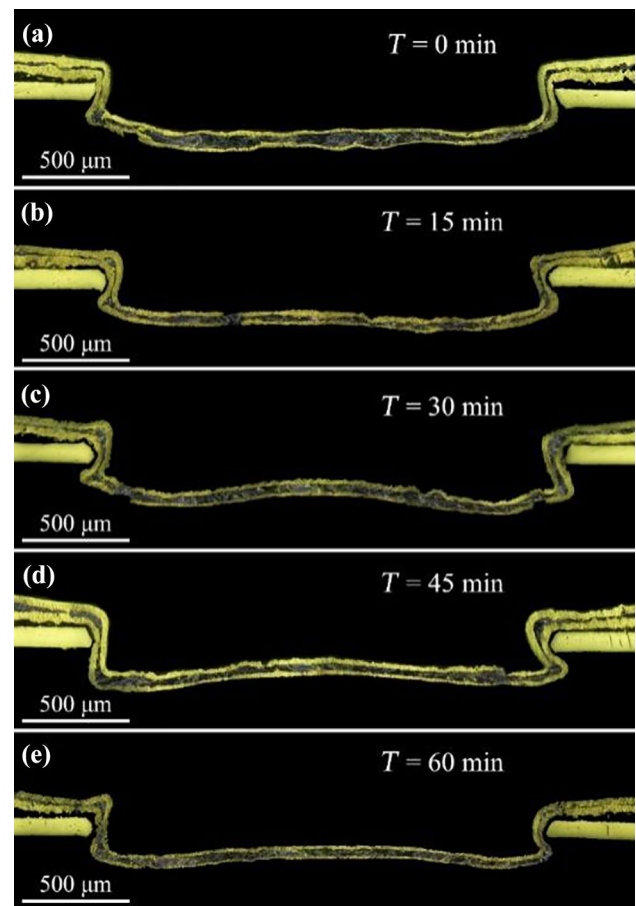


Fig. 12 LSAC joints manufactured under different curing time T : **a** 0 min, **b** 15 min, **c** 30 min, **d** 45 min, **e** 60 min

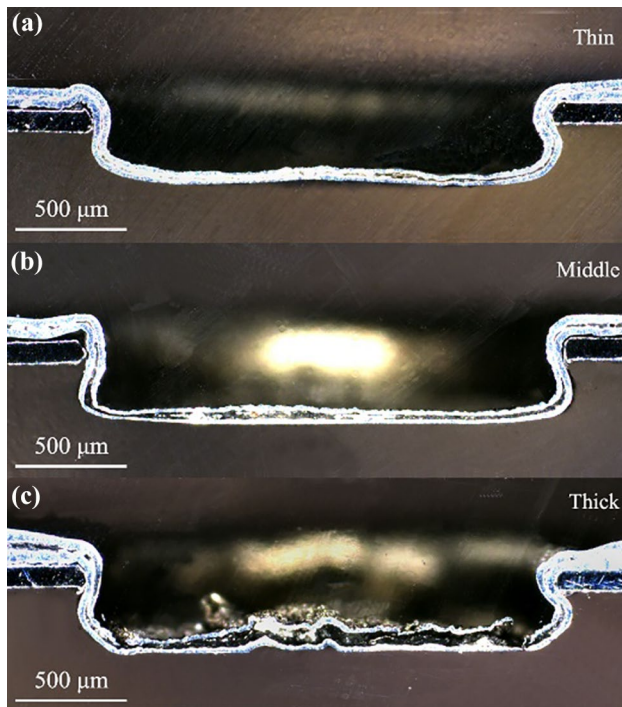
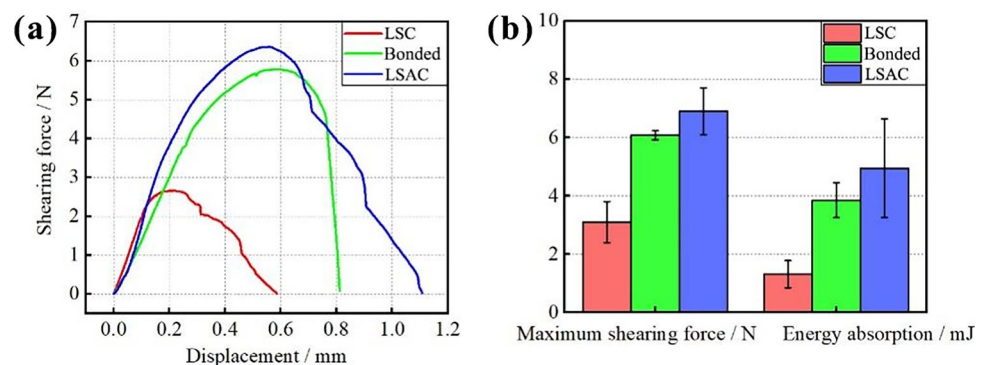


Fig. 13 Section views of hybrid joints with different adhesive layer thicknesses: **a** thin, **b** middle, **c** thick

the joint and bursts the foils at the button corner, as shown in Fig. 13c. Besides, due to structural instability, the interlock structure of the joint in (c) is different from that in (a) and (b). The undercut in (c) locates close to the perforated sheet, while those of (a) and (b) are close to the button bottom. The reason is that the foil at the bottom is not easy to stretch with excessive adhesive, and the interlock structure is mainly deformed by stretching of the sidewall. The adhesive thickness of LSAC joints should be as thin as possible, so that the deformation can be uniform, preventing serve thickness thinning and reducing the size of adhesive pockets.

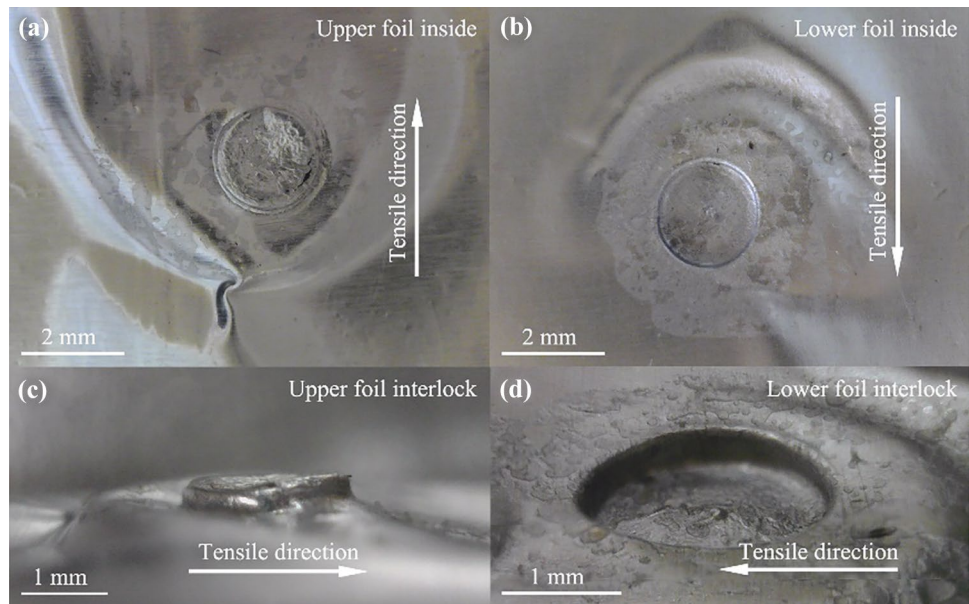
Fig. 14 Shear strength of LSAC joints: **a** force–displacement curves; **b** maximum force and energy absorption



3.3 Strength of LSAC joint

To comprehensively contrast the superiority of LSAC over LSC and adhesive bonding, lap-joint specimens of LSAC, LSC, and bonded joints are made for the shear test. The thicknesses of foil, adhesive layer, and perforated sheet are 30 μm , about 10 μm , and 0.1 mm, respectively; forming height H is 0.3 mm, laser energy E is 280 mJ, laser spot diameter is 5 mm, and laser shock number N is 60. The shear test speed is 1 mm/min. Test results are shown in Fig. 14, where (a) is the shear force–displacement curves of the three joints, and (b) is the maximum shear load and energy absorption. In Fig. 14(a), the peak value of the LSAC joint is a little higher than the bonded joint but significantly higher than the LSC joint. Meanwhile, the curve shape of the LSAC joint is closer to the bonded joint. These phenomena indicate that the shear strength of the LSAC joint is mostly provided by adhesive bonding. In addition, the maximum shear failure distance of the LSAC joint is also larger than the other two kinds of joints, and its curve declines slowly after reaching the peak value, indicating that the failure process is gradually completed, similar to the LSC joint, while the failure of the bonded joint is quite faster and almost instantaneous, which proves that the interlock structure is beneficial to enhance the deformation resistance of joints. Figure 14b contrasts the maximum shear force and energy absorption of the three kinds of joints. The maximum shear force of the LSAC joint is 13.6% higher than bonded joint and 122.0% higher than LSC joint, and the energy absorption is 28.7% and 275.2% higher than bonded and LSC joint, indicating the superiority of LSAC on joint shear strength. However, it is also worth noticing that the two indexes of the LSAC joint have a more serious standard deviation; this is because LSAC is a combination of the two connecting techniques and involves more influence factors, making it harder to control joint connection quality.

Fig. 15 Morphology observation of failed LSAC joint. **a** Upper foil inside, **b** lower foil inside, **c** upper foil interlock structure, **d** lower foil interlock structure



3.4 Failure analysis of LSAC joint

Figure 15 exhibits the morphology of a failed LSAC joint, the adhesive is degummed, the interlock structure is ruined, and the two foils are separated. Residual adhesive can be observed on the inside surfaces of upper and lower foils of a failed LSAC joint, as shown in Fig. 15a and b, but the thickness and distribution of residual adhesive on the two foils are different, indicating that the cohesive failure and interface failure of adhesive occur simultaneously. A distorted interlock structure on the upper foil can be observed in Fig. 15c, while the interlock structure on the lower foil in Fig. 15d is still in good condition; this may be caused by the protection of perforated sheets on the lower foil.

Figure 16 contrasts the simulated and experimental shear test results of the LSAC joint, the simulated result is consistent with the experimental, which proves the reliability of the simulation. According to the curve, the shear force increases rapidly in the range of 0.00 to 0.26 mm displacement. After passing the feature point at 0.26 mm, it continues to increase in the range from 0.26 to 0.41 mm but with a slower growth rate. From the feature point at 0.41 mm, the shear force begins to decrease, two rapid declines of the curve appear at feature points 0.67 mm and 0.82 mm, and finally, the shear failure of the LSAC joint is finished.

Figure 17 shows the simulated structure and morphology of LSAC foil at four feature points during the shear test. The model of the perforated sheet is hidden, and the tensile direction is marked. When the displacement reaches 0.26 mm, some of the adhesives are cohesion-failed at the edge of the joint, and the elements are deleted. When displacement reaches 0.41 mm, the cohesion failure appears at the button corner. When displacement is 0.67 mm, the cohesion failure

of adhesive continues to increase, and plenty of cohesion failures appear at the joint bottom. When displacement is 0.82 mm, the adhesive layer is destroyed, part of the adhesive is separated from the lower foil and remains on the inside surface of the upper foil, and the other adhesive elements are deleted due to cohesion failure. From 0.26 to 0.41 mm, the interlock structure of the LSAC joint has no obvious change. When displacement reaches 0.67 mm, the interlock structure is first destroyed. When the displacement reaches 0.82 mm, the interlock structure near the tensile direction is destroyed, and the whole interlock structure breaks out completely. During the shear process, the two foils are separated, the upper foil is distorted, and the adhesive is destroyed; the lower layer foil has no obvious deformation.

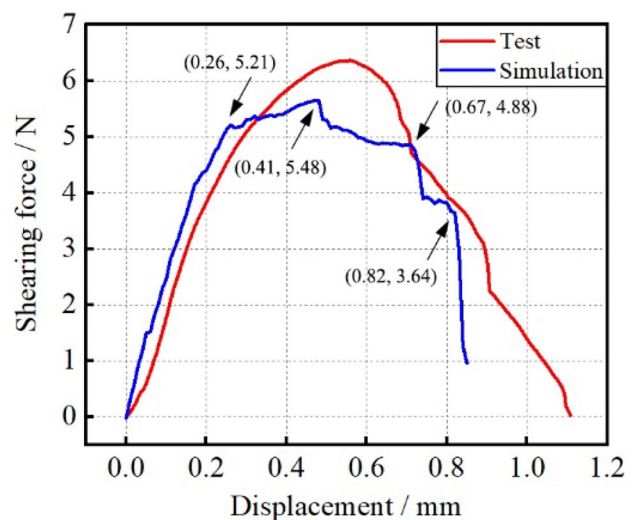


Fig. 16 Experimental and simulated shear test results of LSAC joint

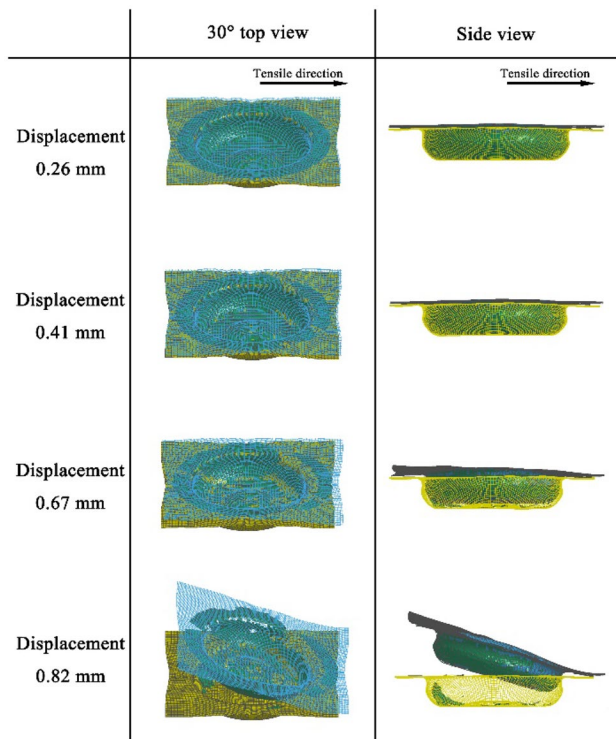


Fig. 17 Simulated results of the four feature points in the LSAC joint shear test

By combining the results in Figs. 16 and 17, it can be concluded that the failure of the adhesive layer mainly occurs from 0.26 to 0.67 mm displacement, while the failure of the interlock structure occurs from 0.67 mm displacement to the end of the test. For the shear failure process of LSAC joints, the adhesive failure occurs first, including cohesion failure and interface failure. Cohesion failure occurs before interface failure, and interlock structure failure occurs after adhesive failure.

4 Conclusion

In this paper, an original process named LSAC is put forward and investigated based on the existing clinch-bonded hybrid joining and LSC techniques, using 1060 aluminum foil, 304 perforated stainless steel sheet, and Henkel EP 5055 structural adhesive. The process of LSAC, the effect of adhesive on LSAC, the joint strength, and the joint failure are investigated through experiments and FEM simulations. The major conclusions are as follows:

1. During the process of LSAC, the most severe thickness reduction of Al foils appeared at the button corner, which suffers high stress concentration. The adhesive tends to redistribute and gathers into little adhesive pockets at the undercut, where the stress level is relatively low

2. The low viscosity adhesive is detrimental to LSAC joint forming when the curing time is less than 15 min. After reaching a certain degree, the adhesive viscosity has little effect on the forming of LSAC joint. An adhesive layer with a thin thickness is beneficial for preventing foil fracture and minimizing adhesive pocket
3. The shear strength of the LSAC joint is mainly provided by adhesive bonding. The shear strength of the LSAC joint is 13.6% and 122.0% higher than pure bonded and pure LSC joints. The shear failure process of the LSAC joint is adhesive degumming first, then the interlock structure separating.

Author contribution All the authors contributed to the study's conception and design. Material preparation, data collection, and analysis were performed by Yiqun Wang. The first draft of the manuscript was written by Yiqun Wang, and all the authors commented on previous versions of the manuscript. All the authors read and approved the final manuscript.

Funding This work is supported by the National Natural Science Foundation of China (Nos. 52075298, 51575314, 51801031, 52075299) and the Fund of the State Key Laboratory of Solidification Processing in NPU (No. SKLSP202014).

Availability of data and materials All data generated or analyzed during this study are included in this published article.

Code availability Not applicable.

Declarations

Ethics approval Not applicable.

Consent to participate The authors declare that they consent to participate in this paper.

Consent for publication This manuscript is approved by all authors for publication.

Competing interests The authors declare no competing interests.

References

1. Mayyas A, Qattawi A, Omar M, Shan DR (2012) Design for sustainability in automotive industry: a comprehensive review. *Renew Sustain Energy Rev* 16(4):1845–1862
2. Taub A, Moor E, Luo A, Matlock D, Speer J, Vaidya U (2019) Materials for automotive lightweighting. *Annu Rev Mater Res* 49(1):327–359
3. Zhang DW, Huang Y (2021) Influence of surface roughness and bondline thickness on the bonding performance of epoxy adhesive joints on mild steel substrates. *Prog Org Coat* 153:106135
4. Peng H, Chen C, Ren XQ, Wu JL (2022) Development of clinching process for various materials. *Int J Adv Manuf Technol* 119:99–117

5. Maggiore S, Banea MD, Stagnaro P, Luciano G (2021) A review of structural adhesive joints in hybrid joining processes. *Polymers* 13(22):3961
6. He XC (2017) Clinching for sheet materials. *Sci Technol Adv Mater* 18(1):381–405
7. Wines B (1989) Adhesive and mechanical clinch bond strengths - a comparison to spot weld strengths. International Congress and Exposition. SAE Technical Paper 890517
8. He XC, Zhao L, Yang HY, Xing BY, Wang YQ, Deng CJ, Gu FS, Ball A (2014) Investigations of strength and energy absorption of clinched joints. *Comput Mater Sci* 94:58–65
9. Lei L, He XC, Zhao DS, Zhang Y, Gu FS, Ball, (2018) Clinch-bonded hybrid joining for similar and dissimilar copper alloy, aluminium alloy and galvanised steel sheets. *Thin-Walled Struct* 131:393–403
10. Balawender T, Sadowski T, Golewski P (2011) Experimental and FEM analyses of clinched and adhesively bonded hybrid joints. *J Adhes Sci Technol* 25:2391–2407
11. Sadowski T, Balawender T (2011) Technology of clinch–adhesive joints. *Adv Struct Mater* 6:149–176
12. Moroni F, Pirondi A, Kleiner F (2010) Experimental analysis and comparison of the strength of simple and hybrid structural joints. *Int J Adhes Adhes* 30:367–379
13. Balawender T, Sadowski T, Kneć M (2011) Technological problems and experimental investigation of hybrid: clinched - adhesively bonded joint. *Arch Metall Mater* 56(2):439–446
14. Pinger T, Bossche NV (2022) On the influence of zinc coating and outdoor exposure on the strength of adhesive, clinched, and hybrid joints of batch hot-dip galvanized steel. *Int J Adv Manuf Technol* 118:4031–4042
15. Calabrese L, Galtieri G, Borsellino C, Bella GD, Proverbio E (2016) Durability of hybrid clinch-bonded steel/aluminum joints in salt spray environment. *Int J Adv Manuf Technol* 87:3137–3147
16. Xing BY, He XC, Feng M (2012) Analysis on influence of adhesive on strength of clinched joints with mathematical statistics. *International Material Review* 26(1):56–59
17. Liu F, He XC, Xing BY (2014) Influence of material property on clinched and hybrid joints performance. *Journal of Hot Work Technology* 43(11):162–165
18. Friedrich S, Georgi W (2013) Gehde M (2013) Hybrid joining technology - a new method for thermoplastic to metal. ANTEC Conference Proceeding 2:1669–1675
19. Friedrich S, Georgi W, Gehde M, Mayr P (2014) Hybrid joining technology - a new method for joining thermoplastic-metal-mixed components. *AIP Conf Proc* 1593:121–127
20. Zhuang WM, Shi HD, Li M (2019) Curing effects on forming and mechanical performance of clinch-adhesive joints of dissimilar materials between AA5754 Aluminum Alloy and Q235 steel. *J Adhes* 95(5–7):577–594
21. Pirondi A, Moroni F (2009) Clinch-bonded and rivet-bonded hybrid joints: application of damage models for simulation of forming and failure. *J Adhes Sci Technol* 23(10–11):1547–1574
22. Balawender T, Sadowski T, Golewski P (2012) FEM analysis and experiments of the clinch-bonded joint subjected to uniaxial tension. *Comput Mater Sci* 64:270–272
23. Sadowski T, Balawender T, Golewski P (2015) Technological aspects of manufacturing and FEM modelling of clinch-adhesive joints. In: *Technological Aspects of Manufacturing and FEM Modelling of Clinch-Adhesive Joints*. SpringerBriefs in Applied Sciences and Technology. Springer: Cham, 2015, pp 1–59
24. Neugebauer R, Israel M, Mayer B, Fricke H (2012) FEM and experimental studies on the clinch-bonding and riv-bonding process. *Key Eng Mater* 504–506:771–776
25. Fricke H, Vallee T, Mayer B (2017) Modelling of industrial hybrid bonding processes considering fluid-structure-interaction. International Conference on Computational Methods for Coupled Problems in Science and Engineering (COUPLED) - VII International Conference on Computational Methods for Coupled Problems in Science and Engineering (COUPLED 2017) Rhodes Island, Greece, 2017
26. Fricke H, Vallée T (2016) FEM modelling of hybrid-bonded joints. *J Adhes* 92(7–9):652–664
27. Ji Z, Liu R, Wang DG, Zhang MH, Su QC (2008) A micro clinching method and its device for joining ultra-thin sheets with pulsed laser. Chinese Patent. ZL200810014018.1
28. Wielage H, Vollertsen F (2011) Undercuts by laser shock forming. *AIP Conf Proc* 1353:1309–1312
29. Veenaas S, Vollersten F (2014) High speed joining process by laser shock forming for the micro range. 6th International Conference on High Speed Forming
30. Veenaas S, Wielage H, Vollertsen F (2014) Joining by laser shock forming: realization and acting pressures. *Production Engineering - Research and Development* 8:283–290
31. Veenaas S, Vollertsen F (2015) Forming behavior during joining by laser induced shock waves. *Key Eng Mater* 651–653:1451–1456
32. Zheng C, Pan CD, Wang JL, Zhao GQ, Ji Z (2020) Mechanical joining behavior of Cu–Fe dissimilar metallic foils in lasershock clinching. *Int J Adv Manuf Technol* 110:1001–1014
33. Wang X, Qiu TB, Shen ZB, Zhang D, Ma YJ, Gu YX, Liu HX (2016) Forming properties of a microscale laser dynamic flexible forming technique. *Mater Manuf Processes* 31(6):745–750
34. Wang X, Zhang D, Gu CX, Shen ZB, Ma YJ, Gu YX, Qiu TB, Liu HX (2015) Micro scale laser shock forming of pure copper and titanium sheet with forming/blanking compound die. *Opt Lasers Eng* 67:83–93
35. Wang X, Li XD, Li C, Shen ZB, Ma YJ, Liu HX (2018) Laser shock micro clinching of Al/Cu. *J Mater Process Technol* 258:200–210
36. Veenaas S, Vollertsen F (2018) Mechanical joining of glass and aluminum. *Key Eng Mater* 767:369–376
37. Veenaas S, Vollertsen F, Czotscher T (2019) Joining by laser induced shock waves of aluminum and plastics. *AIP Conf Proc* 2113:050029
38. Wang XY, Ji Z, Wang JF, You SX, Zheng C, Liu R (2018) An experimental and FEM study on laser shock clinching for joining copper foil and perforated stainless steel sheet. *J Mater Process Technol* 258:155–164
39. Wang XY, Ji Z, Liu R, Zheng C (2018) Making interlock by laser shock forming. *Opt Laser Technol* 107:331–336
40. Wang XY, Ji Z, Zheng C, Liu R (2020) Joining similar and dissimilar material combinations by laser shock forming. *J Manuf Process* 60:318–327
41. You SX, Wang XY, Ji Z, Zheng C, Zhang GF, Liu R (2019) Making line undercut structure by incremental laser shock forming. *Int J Precis Eng Manuf* 20:1289–1296
42. Wang J, Wang YQ, Wang S, Lu GX, Zheng C (2021) Ji Z (2021) Experimental and FEM investigation on incremental laser shock clinching for joining three sheets of copper/aluminum/stainless steel. *Opt Laser Technol* 141:107141
43. Peyre P, Fabbro R (1995) Laser shock processing: a review of the physics and applications. *Opt Quant Electron* 27:1213–1229
44. Johnson GR, Cook WH (1983) A constitutive model and data for metals subjected to large strains, high strain rates and high temperatures. 7th International Symposium on Ballistics, Hague, Netherlands, pp 541–547
45. Henkel AG, Co. KGaA (2014) Technical Data Sheet TEROSON EP 5055

46. Gerstmann T, Awiszus B (2020) Hybrid joining: FEM process development of flat-clinch-bonding. *J Mater Process Technol* 277:116421

Publisher's Note Springer Nature remains neutral with regard to jurisdictional claims in published maps and institutional affiliations.

Springer Nature or its licensor holds exclusive rights to this article under a publishing agreement with the author(s) or other rightsholder(s); author self-archiving of the accepted manuscript version of this article is solely governed by the terms of such publishing agreement and applicable law.